Seasonal current variability on the New Jersey inner shelf

Josh T. Kohut, Scott M. Glenn, and Robert J. Chant
Institute of Marine and Coastal Sciences, Rutgers University, New Brunswick, New Jersey, USA

Received 16 May 2003; revised 7 November 2003; accepted 12 March 2004; published 31 July 2004.

[1] The well-sampled ocean off the coast of New Jersey provides a data-rich environment in which to study ocean current variability over the inner shelf. Using a year-long HF radar data set, complemented with in situ and meteorological observations, the annual- and seasonal-scale variabilities are examined. The hydrographic variability of the inner shelf off New Jersey is largely bimodal between summer stratification and winter mixing. An annual oceanographic and atmospheric data set was separated into these two regimes. The influence of stratification is evident through a relatively steady current response strongly correlated with the wind during the stratified season and a more variable response less correlated with the wind during the mixed season. When the water column is mixed, the influence of the local topography on the surface current variability is dependent on the slope, with a tendency for the variability to be more aligned with steeper topography. *INDEX TERMS:* 6959 Radio Science: Radio oceanography; 4512 Oceanography: Physical: Currents; 4520 Oceanography: Physical: Eddies and mesoscale processes; 4536 Oceanography: Physical: Hydrography; 4572 Oceanography: Physical: Upper ocean processes; *KEYWORDS:* coastal dynamics, HF radar

Citation: Kohut, J. T., S. M. Glenn, and R. J. Chant (2004), Seasonal current variability on the New Jersey inner shelf, *J. Geophys. Res.*, *109*, C07S07, doi:10.1029/2003JC001963.

1. Introduction

[2] The Middle Atlantic Bight (MAB) has been a regional focus of coastal research since the early 1900s. *Beardsley and Boicourt* [1981] present a literature review of the estuarine and coastal circulation studied from Cape Cod, Massachusetts south to Cape Hatteras, North Carolina. Early observations described by *Bigelow* [1933] and *Bigelow and Sears* [1935] show the hydrography of the MAB has a strong seasonal cycle. Typically strong stratification, brought on by warmer temperatures and increased freshwater runoff, exists beginning in the early spring and continuing through the summer. This stratification is broken down in the fall and early winter by strong storms and cooler temperatures. The first dynamical model for the MAB showed a southwest drift of shelf and slope waters from Cape Cod toward Cape Hatteras [*Svedrup et al.*, 1942]. *Beardsley and Winant* [1979] show numerically that the southwest flow of this cold glacial water is primarily driven as a boundary current connected to the larger-scale circulation of the western North Atlantic Ocean. *Chapman and Beardsley* [1989] also suggest that the origin of the shelf water is from glacial melt along the southern Greenland coast that flows south to the MAB as a buoyant coastal current. Early on, *Miller* [1952] found that there was strong variability about this mean drift in the form of eddies and current filaments. Improved technology enabled more long-term measurements of currents, water temperature and salinity, and meteorological forcing in the 1960s. *Beardsley and Boicourt* [1981] describe much of the work from these longer time series, confirming that transient currents modulate the mean southwest drift.

[3] The focus of dynamical research in the 1970s shifted from the mean southwest flow to the current variability. *Beardsley et al.* [1976] suggest that the current variability of the MAB is mostly wind-driven. *Saunders* [1977] shows that the wind forcing driving this variability is predominately from the west/northwest except in the summer months when the wind is typically from the southwest. The typical timescale of the wind forcing is on the order of 2–10 days [*Moores et al.*, 1976]. On the basis of observations, *Ou et al.* [1981] suggest that the variability is composed of a wind forced component and a larger-scale free wave component that is not correlated with the wind and propagates downshelf. Modeling studies also suggest that these current fluctuations do have a local and nonlocal response. The local response is related to local geometry, topography and forcing and the nonlocal response is due to forcing "distant in time and space" [*Beardsley and Haidvogel*, 1981].

[4] More recent work in the MAB focused on the locally forced variability, particularly in the summer months when the water column is strongly stratified. The strongest signal typically observed along the New Jersey coast during the summer stratification season is coastal upwelling/downwelling. Traditionally, upwelling studies have focused on eastern boundaries such as the Peruvian coast [*Brink et al.*, 1980], coastal waters off California [*Narimousa and Maxworthy*, 1987] and Oregon [*Halpern*, 1976] as well as western Africa [*Halpern*, 1977]. A series of observational and numerical studies of the coastal ocean focused on the region off the Northern California coast [*Beardsley and Lentz*, 1987]. The Coastal Ocean Dynamics Experiment

0148-0227/04/2003JC001963$09.00

(CODE) looked at both the local and regional response of the coastal ocean to atmospheric and freshwater forcing. *Davis and Bogden* [1989] describe the difference seen in the current response over a deep (greater than 60 m) and shallow (less than 60 m) shelf. They suggest that the geostrophic response seen over the deep shelf breaks down over the shallow shelf where frictional surface layers extend all the way to the bottom. More recently, upwelling regions on the eastern continental coasts have been identified. These include the coast of Nova Scotia [*Barth*, 1994] and the North Carolina coast [*Austin*, 1999].

[5] The shelf waters off the New Jersey coast offer a slightly different context to study upwelling. Most of the upwelling research outlined above has focused on regions with narrow continental shelves adjacent to very deep slope waters. The shelf waters off the coast of New Jersey, on the other hand, are characterized by a relatively wide continental shelf with slope waters about 200 km offshore. The strong summer stratification over the shallow shelf complimented with generally alongshore winds make this region subject to frequent upwelling/downwelling events. Using 50 years of temperature data from Cape Cod to the Florida Keys, *Walford and Wicklund* [1968] describe a cold pool of water on the MAB continental shelf. The cell, which is composed of water less than 8°C, is trapped below the thermocline by the highly stratified ocean during the spring and summer [*Houghton et al.*, 1982; *Hicks and Miller*, 1980]. *Hicks and Miller* [1980] also observed that meteorological forcing, if persistent, has the potential to move the western boundary of the cell nearshore and surface along the New Jersey coast. After the annual cycle, the largest fluctuation in sea surface temperature along the New Jersey coast is due to coastal upwelling/downwelling (S. M. Glenn et al., Biogeochemical impact of summertime coastal upwelling in the Mid-Atlantic Bight, submitted to *Journal of Geophysical Research*, 2003, hereinafter referred to as S. M. Glenn et al., submitted manuscript, 2003). While the upwelling observed along the New Jersey coast may initially appear uniformly distributed, after a period of days the cold water develops into distinct upwelling centers. Along the southern New Jersey coast, three upwelling centers develop about 50 km apart and are collocated with three areas of recurrent bottom hypoxia [*Glenn et al.*, 1996]. Using numerical models [*Glenn et al.*, 1996] and analytical simulations [*Song et al.*, 2001], both with ideal topography, the recurrent upwelling centers are shown to be the direct result of the interaction of surface wind forcing and local bathymetry. The centers are found both in models and observations to form on the downwind side of topographic highs and are composed of a nearshore cyclonic circulation cell bounded by the coast onshore and a downwind alongshore jet offshore [*Glenn et al.*, 1996; *Song et al.*, 2001]. One recurring center forms in this study site offshore of Tuckerton, New Jersey.

[6] Additional research in this region has looked at both the sea level and current response to short wind events during the highly stratified summer season. For example, *Yankovski and Garvine* [1998] document a strong interaction between the wind-forced response and a coastal buoyant jet driven by fresh Hudson River outflow during a very wet year. They describe an intensification of the wind-driven currents in the buoyant water as it extends offshore. Additionally, *Münchow and Chant* [2000] show that the vertical and horizontal variability of the subinertial response to an alongshore wind stress are characterized by a coupling between wind forced and buoyancy regimes that rotates counterclockwise with depth. *Chant* [2001] focuses on the near-inertial band of the wind driven response. The energy within this band is initially uniform across the surface and propagates into the thermocline within two inertial periods.

[7] This paper examines the local response of the surface current fields to the local wind forcing over longer seasonal scales. As the summer months pass and the cold winter sets in, the stratification sharply decreases and the forcing changes from light summer breezes to strong winter storms. This study uses spatial time series observations from an HF radar and a bottom-mounted ADCP to describe the structure of the three-dimensional response to local forcing. Since stratification varies significantly on seasonal scales, analysis is performed separately on stratified and unstratified conditions. The role of the local forcing and topography also influence the local dynamics on seasonal timescales.

2. Instrumentation

[8] The 25 MHz CODAR-type HF radar network deployed around Tuckerton consists of two remote sites located in Brant Beach and Brigantine, New Jersey (Figure 1). Using Doppler theory, each site measures the radial components of the ocean surface velocity directed toward or away from the site [*Crombie*, 1955; *Barrick*, 1972; *Barrick et al.*, 1977]. Since the systems are using surface gravity waves to estimate these velocity components, the measured currents at this frequency are the weighted average of the currents within the upper one meter of the water column [*Stewart and Joy*, 1974]. The sites were first deployed along the southern New Jersey coast in May 1998 as part of a coastal predictive skill experiment. Since this 3-month test deployment, the two sites were redeployed in May 1999 and continue to operate in real-time. Radial component velocities measured at the two sites are combined into hourly total surface current maps. The dynamical study discussed here focuses on surface fields measured between May 1999 and May 2000. This time span was selected because it includes periods with both strongly stratified and mixed water columns and the stratified period is subject to several upwelling/downwelling events. In addition, the spring and summer of 1999 were anomalously dry, minimizing the freshwater contribution to the local circulation.

[9] All data were processed using measured antenna beam patterns as described by *Kohut and Glenn* [2003]. This technique was demonstrated to produce the best comparison with concurrent in situ current meter data. The radial data were combined into hourly averaged total vector maps on a fixed grid using the CODAR Ocean Sensors software package. The entire record at each grid point was detided using a least squares fit of the five strongest constituents (M_2, S_2, N_2, K_1, and O_1) to the raw time series data. The subtidal data were then low-pass filtered with a cutoff period of 30 hours. The surface data used in this study only included grid points that had at least 70% return over the annual record (Figure 2). The Geometric Dilution of Precision (GDOP) describes the spatial error

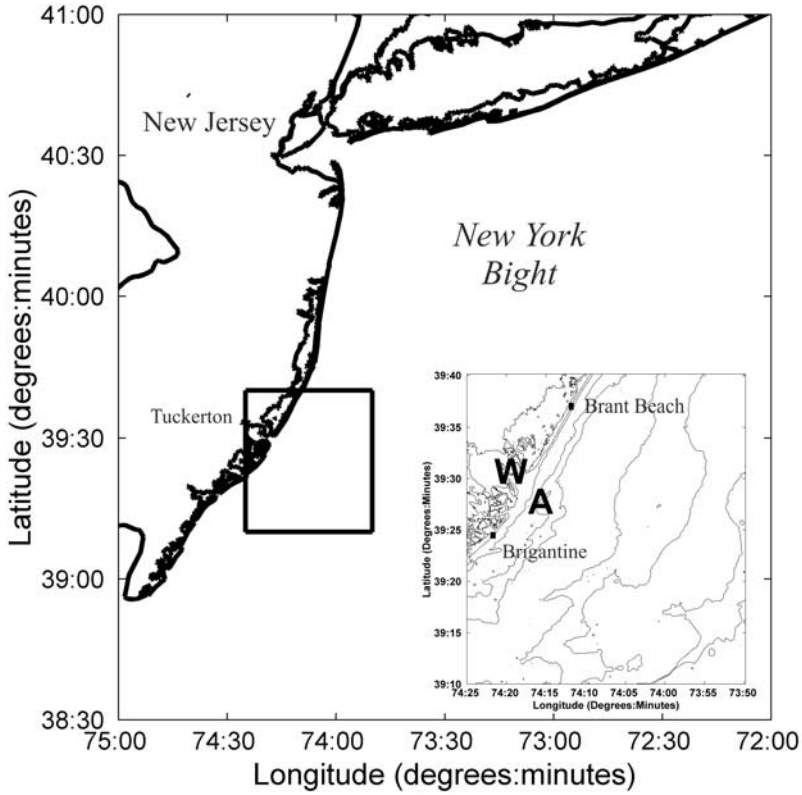

Figure 1. Map of the research area. The locations of the HF radar sites (solid squares), ADCP (A) and meteorological station (W) are shown in the inset. The 5 m depth contours range from 5 m nearshore to 35 m offshore.

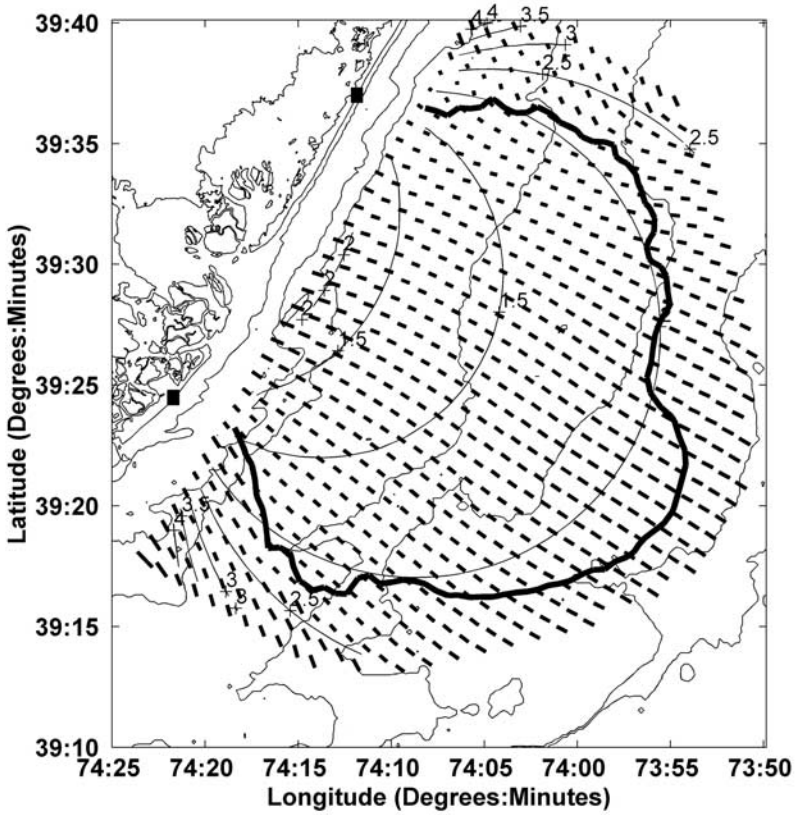

Figure 2. The GDOP contours (thin) of the HF radar system, tidal ellipses for the M2 constituent, and the 70% coverage contour (thick) of the annual data set.

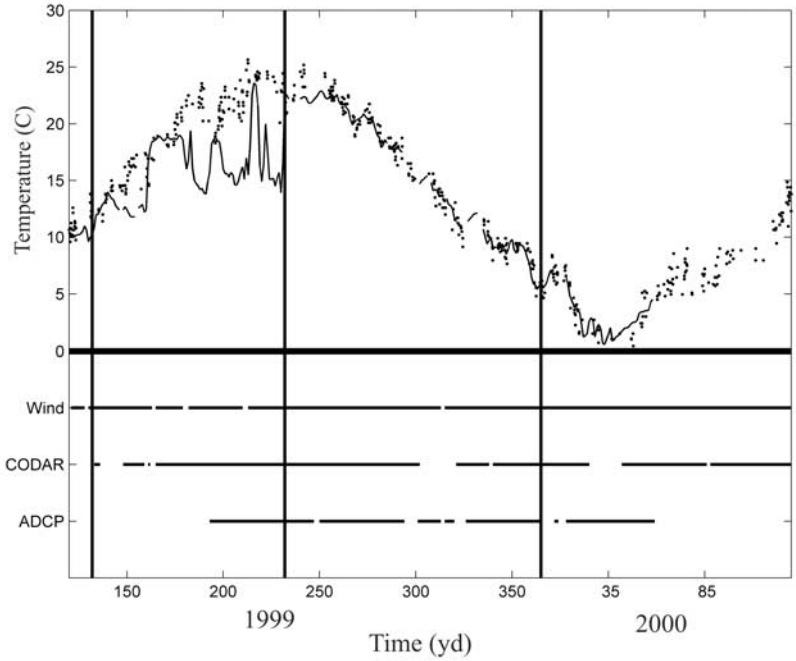

Figure 3. Time series of sea surface temperature (dots), bottom temperature (solid line), and the availability of wind velocity, HF radar, and ADCP data. The stratified and mixed regimes are delineated by vertical lines.

associated with the geometric combination of the radial velocity measurements [*Chapman et al.*, 1997]. The specific GDOP for this HF radar setup indicates that the geometric error increases rapidly toward the northwest and southwest nearshore corners of the coverage (Figure 2). The selected 70% coverage area is within GDOP values of 2.5 or less. The tidal estimates from the detiding step were used to further verify the data quality of the selected grid since the orientation of the major axis of the tidal ellipse should not vary significantly over the grid [*Battisti and Clarke*, 1982]. The M_2 tidal ellipses (Figure 2) confirm that areas in which the major axes vary are collocated with larger GDOP, indicating that these regions contain less reliable total vectors. Since the data within the 70% contour has low GDOP and consistent tides, these data were used in the following analysis.

[10] Complimentary in situ data were obtained from the Long-term Ecosystem Observatory (LEO) [*Grassle et al.*, 1998; *Glenn et al.*, 2000; *Schofield et al.*, 2001], located midway between the two CODAR sites (Figure 1). Remotely operated profilers that sample subsurface properties (including temperature, salinity, and pressure) and a bottom mounted Acoustic Doppler Current Profiler (ADCP) are located about 5 km offshore in 12 meters of water (Figure 1). Using a least squares fit, the ADCP data was detided using the M_2, S_2, N_2, K_1, and O_1 constituents to match the CODAR data processing. A meteorological tower at the Rutgers University Marine Field Station compliments the ocean observations with a suite of atmospheric data. Satellite imagery obtained from the Rutgers University Coastal Ocean Observation Lab provides continuous spatial coverage of sea surface temperature over the region. This particular study utilizes surface map time series of currents and temperature from the HF radar and satellites, bottom temperature and subsurface ADCP velocity profiles from LEO, and local wind measurements from the meteorological tower (Figure 3). The detided ADCP and wind data were centered averaged on the hour and filtered to match the HF radar sampling.

3. Results

3.1. Annual Mean

[11] The annual mean between May 1999 and May 2000 is a relatively weak flow generally alongshore toward the southwest (Figure 4). While consistent with historical results, the surface flow is clearly influenced by the underlying topography. On the northern side of the domain, the topography is relatively deep and flat rising sharply at the beach. On the southern side, however, steep rises are encountered offshore between 20 m and 25 m and again between 15 m and 10 m. The resulting topographic bump is also the site of numerous kilometer-scale shore oblique sand ridges. Southward heading flows thus encounter isobaths that veer offshore in the center of the domain. The flow generally follows these isobaths, veering offshore and accelerating. Downstream of the topographic bump the flow returns to an alongshore direction. The HF radar field indicates that on annual timescales, the surface currents are significantly influenced by local topography on the order of the baroclinic Rossby radius $O(10$ km). In the absence of stratification, surface and bottom boundary layers will often overlap in coastal ocean water depths less than 30 m [*Brink*, 1997]. Topographic steering of the annual mean flow indicates that this timescale may be influenced by a longer unstratified season during which the entire water column is dominated by coupled surface and bottom boundary layers. Here we discuss the role of stratification

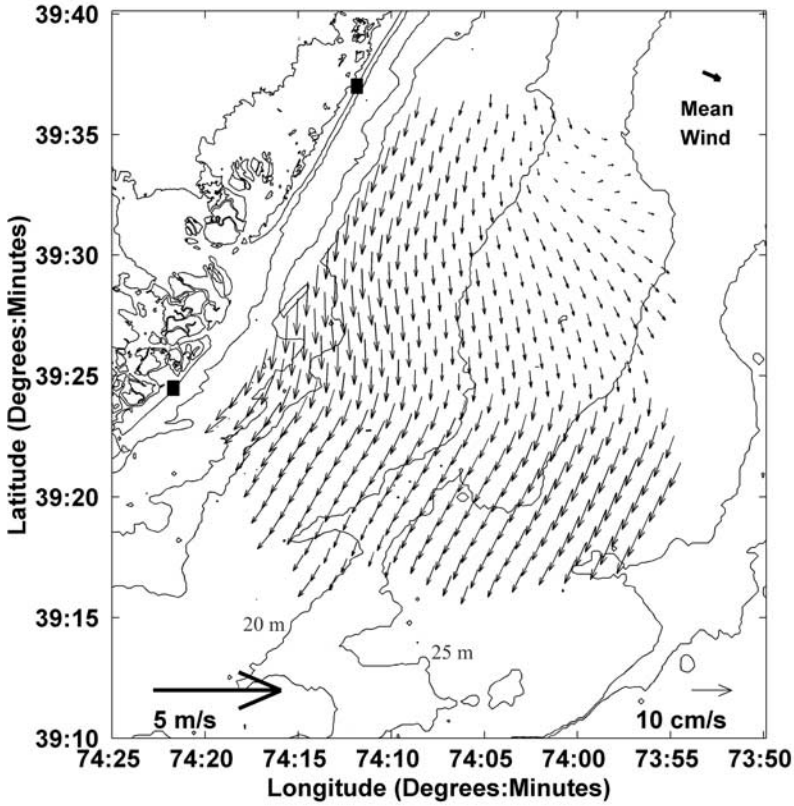

Figure 4. Annual mean currents measured between May 1999 and May 2000 with the HF radar system. The mean wind measured at the marine field station (upper right), the current scale (lower right), and wind scale (lower left) are also shown.

on the interaction and how this interaction influences the current response on seasonal timescales.

3.2. Mixed Versus Stratified

[12] To see the effect of stratification on the surface current field, the annual record was divided into two regimes, stratified and mixed. The stratification was quantified using the surface temperature from a satellite advanced very high resolution radiometer (AVHRR) and the bottom temperature from the LEO SeaBird conductivity-temperature-depth (CTD) sensor. The AVHRR data used here are a subset of a nine year time series (S. M. Glenn et al., submitted manuscript, 2003). The data in this subset were collected locally from the NOAA 12, NOAA 14, and NOAA 15 satellites at the Rutgers University remote sensing lab. Sea surface temperatures were derived from the AVHRR data using the MultiChannel Sea Surface Temperature (MCSST) algorithm [*Bernstein*, 1982]. Any grid point more than 4 degrees different than the surrounding points was eliminated to remove the effect of clouds. All images were manually navigated to approximately one pixel in error. For this analysis the pixel directly over the LEO node was used for the SST time series.

[13] Within the annual data there are two clear regimes, one with significantly different surface and bottom temperatures, labeled stratified, and one with very similar surface and bottom temperatures, labeled mixed (Figure 3). The transition from stratified to mixed is usually associated with a September mixing storm. For this particular year, the stratified regime runs from year-day (yd) 133 to yd 231 and the mixed regime runs from yd 232 to yd 365. Both the current and wind data were divided into these two seasonal regimes so that the influence of stratification on the surface current fields could be studied.

3.3. Stratified Regime

3.3.1. Forcing

[14] The forcing during the summer-stratified season is typically driven by winds and buoyancy. Using the techniques described by *Yankovski and Garvine* [1998], the influence of buoyancy in the research area was determined by the magnitude of freshwater outflow leaving the Hudson River. *Yankovski and Garvine* [1998] describe an approximate 40-day lag between freshwater outflow at Watertown, New York and arrival off the southern New Jersey coast. On the basis of this 40-day lag, the brackets of Figure 5 indicate the freshwater outflow at Watertown, NY that would influence the dynamics of the stratified regime in southern New Jersey. Unlike the spring of 1996 with many record or near record high outflows, the spring of 1999 is characterized by many record or near record low outflows of fresh Hudson River water (Figure 5). The average outflow affecting the circulation during the stratified regime was 187 m^3/s in 1999 and 467 m^3/s in 1996. The summer stratification season of 1999 is likely to have a much smaller buoyant forced response than that observed in previous years.

[15] The wind forcing during the stratified regime was strong and predominantly alongshore. A histogram of the

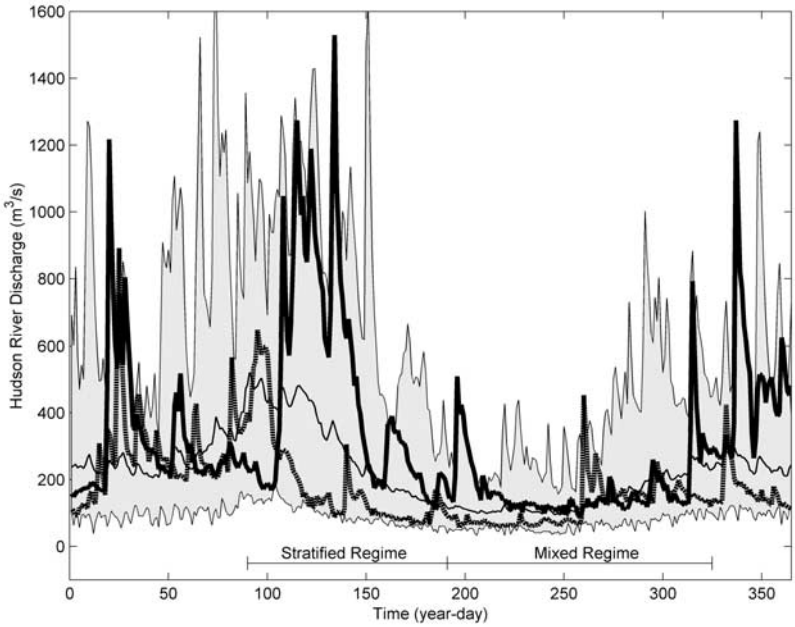

Figure 5. The daily averaged Hudson River outflow for 1996 (thick) 1999 (dashed), and the 25 year mean (thin) measured at a USGS station near Watertown, New York. The 25 year data envelope is shaded.

low-passed filtered winds shows that the wind was mostly from the northeast (downwelling favorable) and the southwest (upwelling favorable) with the southwest winds dominating (Figure 6). The mean and standard deviation of the wind velocities from each direction indicates that the strongest velocities with the most variability were from the upwelling favorable direction. The forcing of the 1999 summer stratification season was dominated by an oscillation between upwelling and downwelling favorable winds.

3.3.2. Response

[16] The current response during the stratified regime was separated into a mean and transient using a Reynolds decomposition approach, U = Ubar + U′, so that Ubar is the mean and U′ is the transient. The mean response is relatively weak across the field with an average magnitude of 3.6 cm/s (Figure 7a). The current direction varies significantly across the field and indicates a weak relationship with the mean southwesterly alongshore wind. The

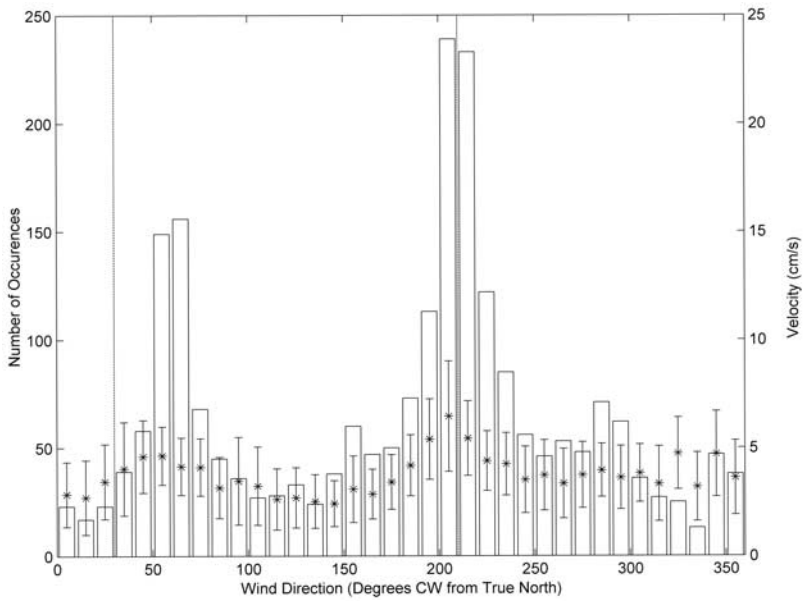

Figure 6. Histogram of wind forcing over the stratified regime. The mean (stars) and standard deviation (bars) of the wind velocity in each angular bin are also shown. The dashed lines indicate the bearing of the coast to the north and south.

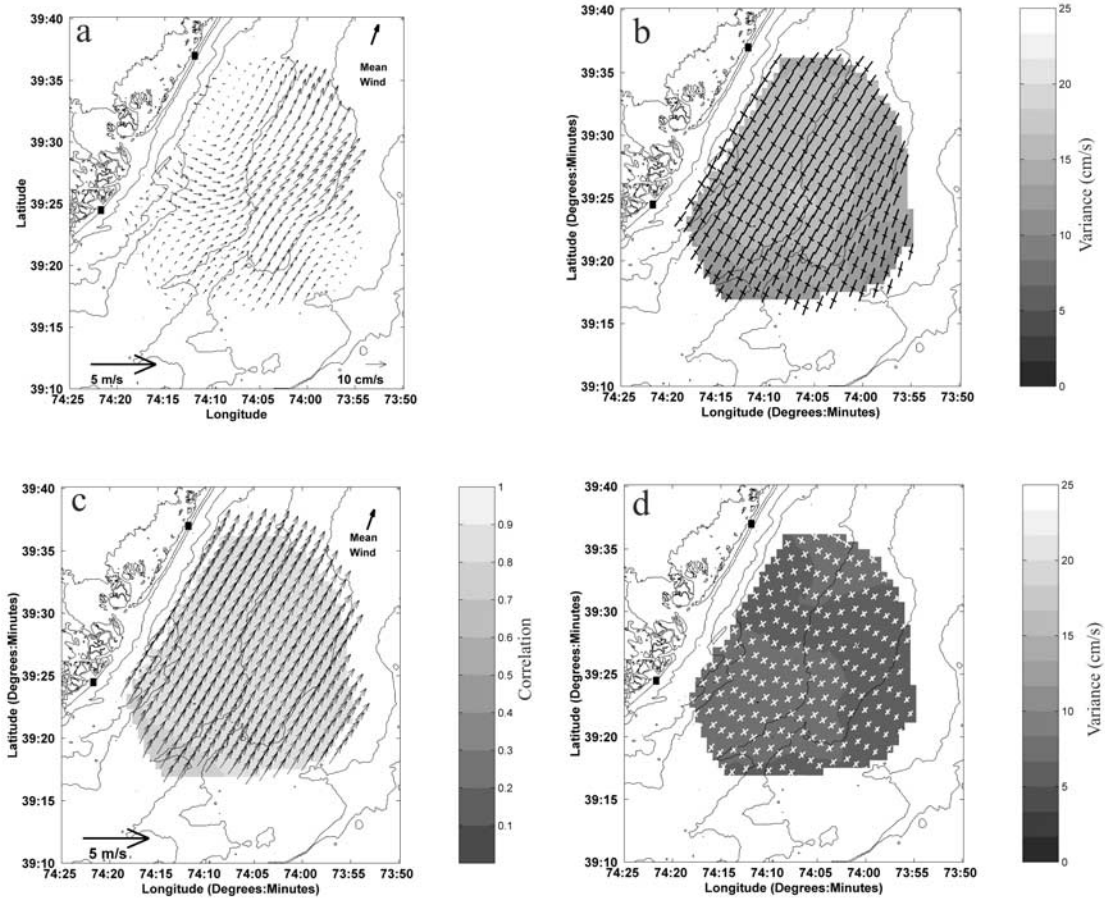

Figure 7. (a) The mean stratified regime current response. The mean stratified wind measured at the field station (upper right), the current scale (lower right), and wind scale (lower left) are also shown. (b) Principle components of the stratified regime transient response. (c) The magnitude of the complex correlation of the stratified regime transient current response with the local winds is shaded. The angle between the mean wind (upper right) and each grid point (black vectors) indicates the offset between the highest correlated current and wind. (d) Variance of the uncorrelated current component of the stratified regime transient response.

cyclonic rotation north of the bump hints at the interaction between surface currents and topography described by *Glenn et al.* [1996] and *Song et al.* [2001]. The transient, on the other hand, is fairly uniform and much more energetic (Figure 7b). The principle components are strongly rectilinear indicating a tendency for the variability to be aligned with the coast. This combined with a weak mean indicates that over the entire stratified regime the response is highly variable in magnitude but tends to be oriented along the coast.

[17] The complex correlation between the local wind time series and the transient current response at each HF radar grid point shows a very strong correlation, with a mean of 0.82, a mean range of ±0.065 for the 95% confidence interval, and a standard deviation of 0.05 across the entire field (Figure 7c). In addition to the magnitude, the vectors indicate that the current direction with the highest correlation is shifted to the right of the wind. This offset fluctuates slightly across the field with a maximum of 23 degrees at the center of the field, a minimum of 4 degrees near the northern edge, and a mean of 14.2 degrees. The vertical variability of this correlation was determined from the ADCP. As expected, the surface currents are more correlated with the wind than the bottom currents (Figure 8). The phase indicates that the highest correlated currents are shifted to the right of the wind at the surface and rotate to the left with depth. The spiral is a fairly typical picture of an upwelling/downwelling regime in which the surface layer moves to the right of the forcing and the bottom layer moves to the left.

[18] A linear correlation was used to identify that component of the observed flow most correlated with the wind. The complex correlation between the wind and each HF radar grid point indicates the magnitude and direction between the best correlated wind and current response. For each grid point, the wind was rotated according to the complex correlation and a best fit-linear regression was used to describe the relationship between the wind and current so that:

$$u_{cor}(x,y,t) = slope_x(x,y)*u_{wind}(t) \quad (1)$$

$$v_{cor}(x,y,t) = slope_y(x,y)*v_{wind}(t) \quad (2)$$

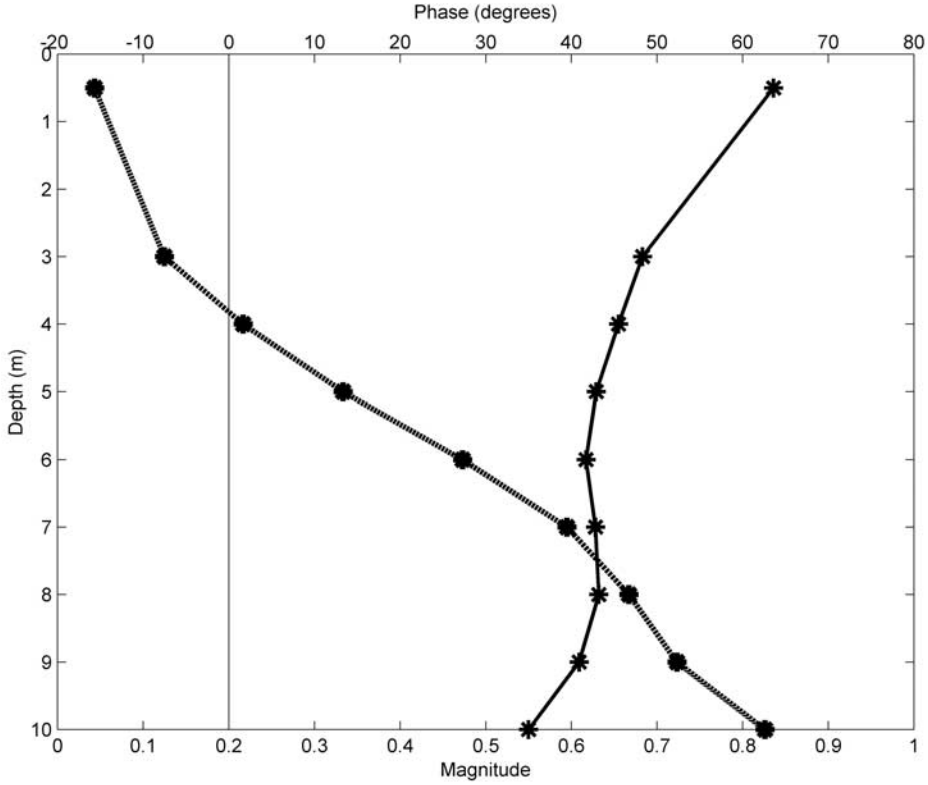

Figure 8. Magnitude (thick) and phase (dashed) of the complex correlation between the vertical current profile and the local wind forcing during the stratified regime. The markers indicate the centers of the measurement bins for the ADCP and CODAR (surface). Negative phase indicates that the highest correlated current is to the right of the wind. The thin line indicates zero phase.

where $slope_x$, and $slope_y$ are the slopes of the linear fit for the east and north current components, respectively. The predicted flow, u_{cor} and v_{cor}, are the east and north components of the wind-correlated current. If this correlated response is subtracted from the total response, the residual is labeled the component of the flow uncorrelated with the wind.

$$u_{total} = u_{cor}(x, y, t) + u_{uncor}(x, y, t) \tag{3}$$

$$v_{total} = v_{cor}(x, y, t) + v_{uncor}(x, y, t) \tag{4}$$

[19] The magnitude of this uncorrelated current for each directional component, u_{uncor} and v_{uncor}, is a function of the scatter about the linear fit (Figure 9). The variance of the current uncorrelated with the wind is significantly less than the total variance (Figure 7d). Therefore the wind forcing accounts for the majority of the variability seen in the stratified transient response. This indicates a tightly linked system between the wind forcing and the current response. Since the orientation of the forcing and response are both along the coast, a better representation of the current structure related to the local forcing can be achieved by separating the stratified regime into upwelling and downwelling regimes.

3.3.3. Upwelling Regime

[20] The mean surface response during upwelling favorable winds is, as expected, up-shelf and shifted to the right of the wind. (Figure 10a). Nevertheless, an interesting spatial variability exists in this mean upwelling response that is more evident after subtracting the spatial mean from each vector (Figure 10b). The spatial variability in the mean flow during upwelling favorable conditions is characterized by an eddy like feature that rotates cyclonically immediately north of the topographic high.

[21] This flow variability is similar in structure to the circulation observed when upwelling winds relax as described by R. J. Chant et al. (Flow reversals during upwelling conditions on the New Jersey inner shelf, submitted to *Journal of Geophysical Research*, *109*, 2003) and *Chant* [2001]. The recirculation north of the bump would advect with it the cool upwelled water along the coast, move it offshore in the vicinity of LEO, and feed a growing upwelling center. The eddy location also coincides with numerical results in which the upwelling center north of the bump is characterized by a cyclonic eddy [*Glenn et al.*, 1996] within an upwelling center.

3.3.4. Downwelling Regime

[22] The mean surface response to downwelling favorable winds is again relatively strong (Figure 11a). The horizontal shear of the downwelling regime is more uniform than the upwelling regime and appears to be related to the stratification (Figure 11b). During a typical downwelling event, the thermocline intersects the bottom. Offshore of this intersection the water column remains stratified, while onshore of the intersection the water column becomes mixed. The spatial structure of the mean can also be

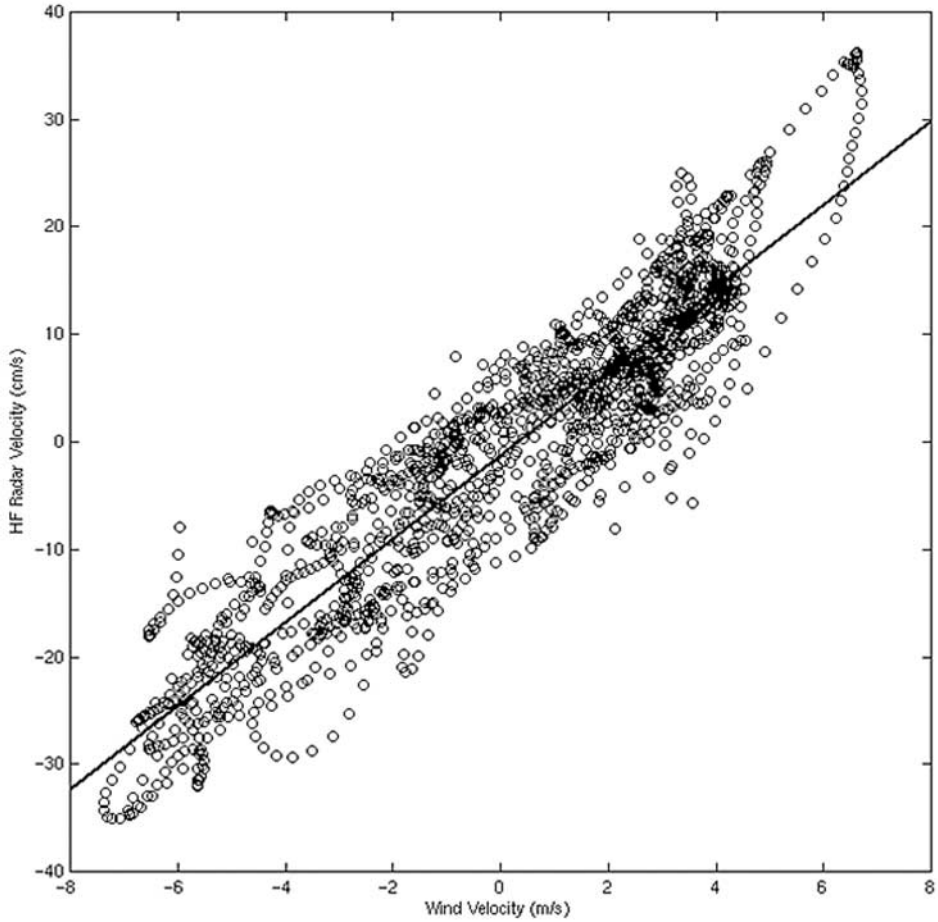

Figure 9. Scatterplot of wind and surface velocity for a single HF radar grid point. The line indicates the slope used to predict the wind-correlated component of the flow.

separated into two regions. The nearshore response of the mixed region is alongshore toward the south and oriented to the left of the wind (Figure 11b). The convergence zone in the southwest sector of the coverage is indicative of an acceleration of the flow over the bump and deceleration downwind of the bump. The offshore response of the stratified region, no longer oriented with the coast, is more closely aligned with the wind.

[23] When the current response is divided into upwelling and downwelling regimes, relatively strong means and weak variability result. In both responses the nearshore region is more influenced by topography where stratification is reduced.

3.4. Mixed Regime

3.4.1. Forcing

[24] The buoyancy forcing during the mixed regime was again below the 25 year mean through much of the time period (Figure 5). The peak seen around yd 260 in the Watertown outflow is from a large rain event associated with the passing of tropical storm Floyd. While Floyd was a significant freshwater event, over the seasonal scale studied here the influence of the buoyancy is relatively low. Similar to the stratified regime, the contribution of buoyancy to the local circulation is assumed small relative to that of the local wind forcing.

[25] The wind forcing throughout the mixed regime was much more evenly distributed than observed during the stratified regime with a peak in the northwest direction (Figure 12). This is consistent with the climatology described by *Saunders* [1977] in which the winds measured over much of the year tend to be from the northwest. The mean and standard deviation of the wind measured in each directional bin show that the forcing is stronger and more variable than observed in the stratified regime (Figures 12 and 6).

3.4.2. Response

[26] The mean response closely resembles that seen in the annual mean (Figures 4 and 13a). Again the currents follow the local topography north of the bump and turn more alongshore south of the bump. The magnitude of the flow is on the order of 4.5 cm/s. The spatial structure of the variance also reflects the underlying topography with an energy maximum centered over the bump (Figure 13b). The mean and transient indicate that the response is relatively steady surrounding the bump and much more variable over the bump.

[27] Correlation between the wind forcing and this response indicate the current is now less correlated with the wind than during the stratified regime, with a mean of 0.69, a mean range of ±0.09 for the 95% confidence interval, and a standard deviation of 0.03 across the field. The vectors

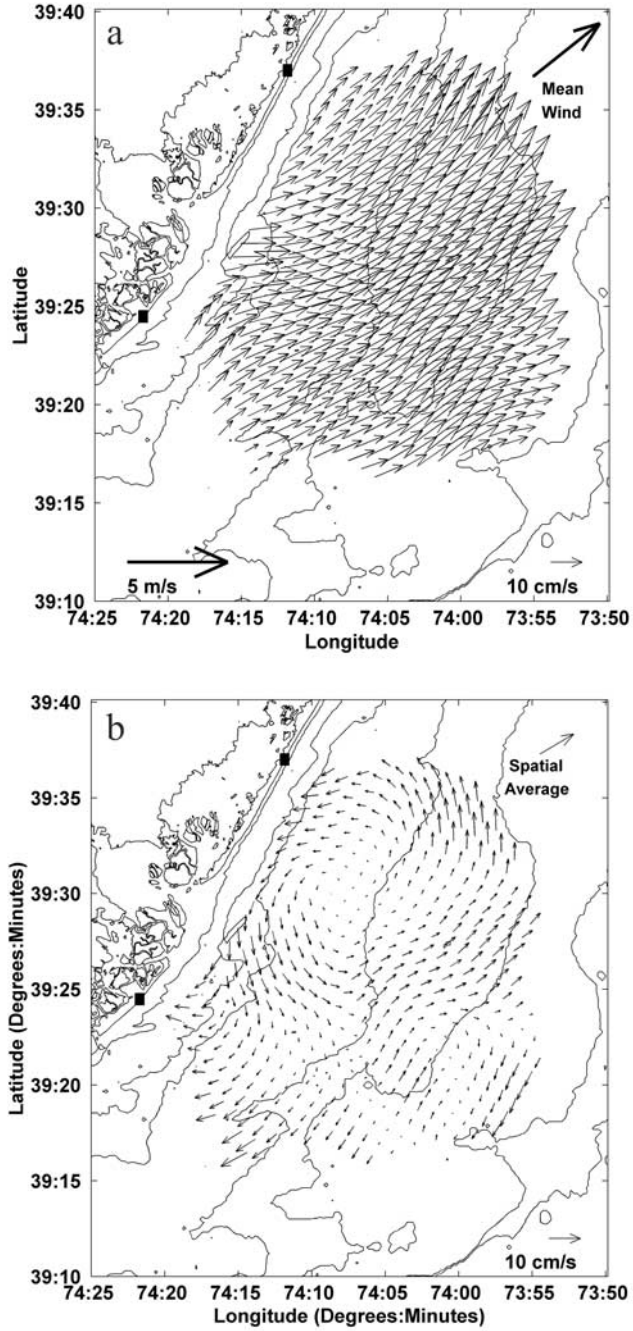

Figure 10. (a) Mean upwelling regime response. The mean upwelling wind measured at the marine field station (upper right), the current scale (lower right), and wind scale (lower left) are also shown. (b) Spatial structure of the mean upwelling response. The vector field is the difference between the temporal mean at each grid point and the spatial mean (upper right).

indicate that the angular offset between the wind and the currents with the highest correlation is now shifted to the left of the wind, with a mean of 14.9 degrees and a maximum of 31 degrees nearshore (Figure 13c). The vertical structure of the correlation at the ADCP is highest at the surface and decreases with depth (Figure 14). The angular shear from surface to bottom is relatively small suggesting that the system is acting as a single layer. The single layer rotation to the left could be an indication of a bottom Ekman layer extending to the surface. Assuming a standard linear eddy viscosity, $K = \kappa u^* z$ [*Smith and Long*, 1976; *Forristall et al.*, 1977], the scale height of the bottom boundary layer for geophysical flows is:

$$l = \frac{\kappa u*}{f} \tag{5}$$

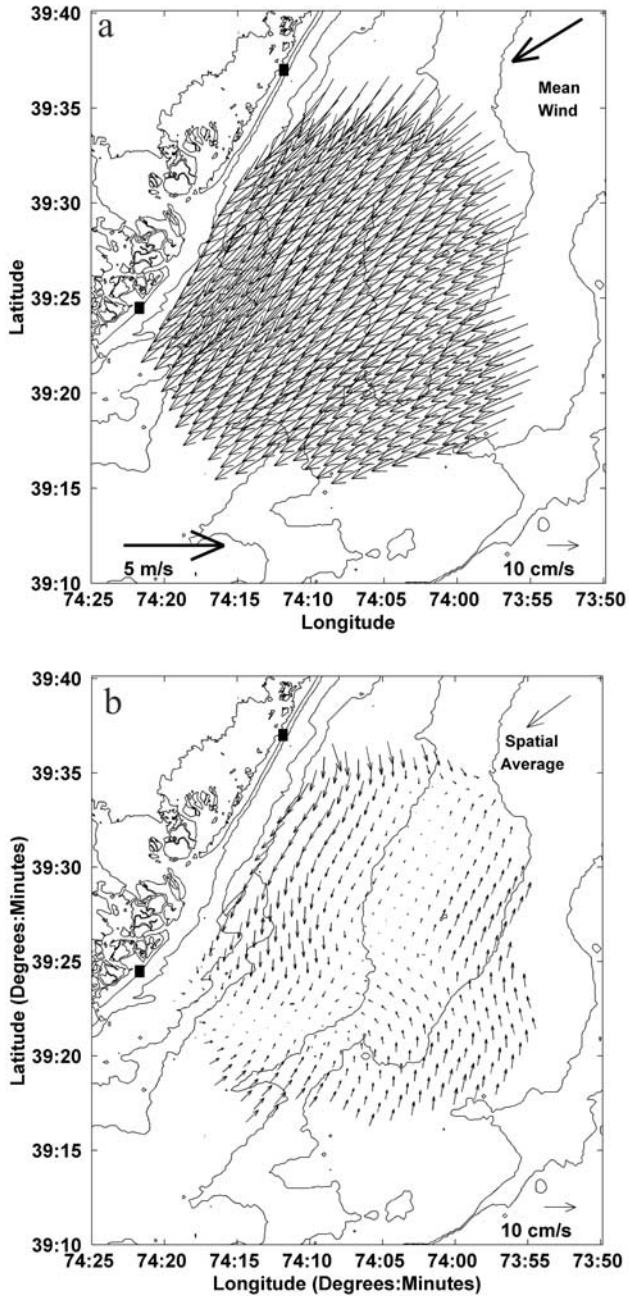

Figure 11. (a) Mean downwelling regime response. The mean downwelling wind measured at the field station (upper right), the current scale (lower right), and wind scale (lower left) are also shown. (b) Spatial structure of the mean downwelling response. The vector field is the difference between the temporal mean at each grid point and the spatial mean (upper right).

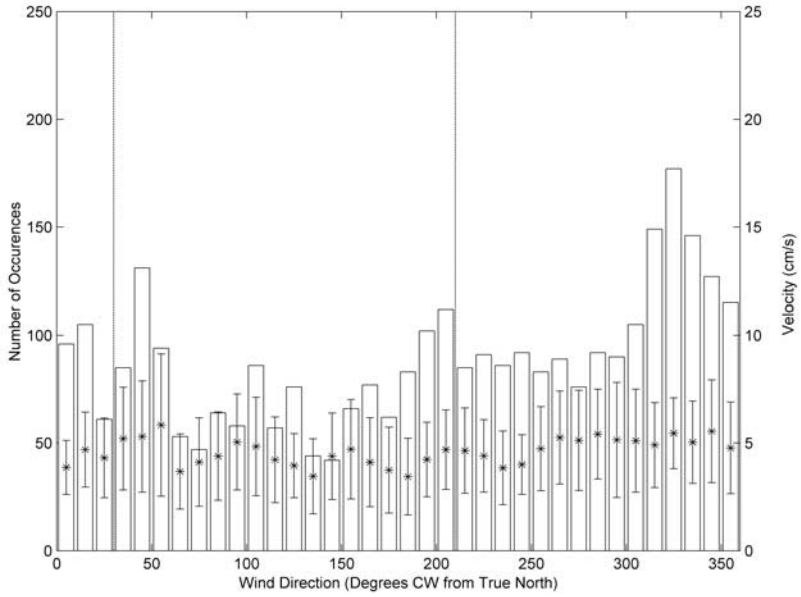

Figure 12. Histogram of wind forcing over the mixed regime. The mean (stars) and standard deviation (bars) of the wind velocity in each angular bin are also shown. The dashed lines indicate the direction of coast to the north and south.

where κ is von Karman's constant, u^* is the frictional velocity, and f is the Coriolis parameter [*Long*, 1981; *Glenn*, 1983]. Since κ and f are constants, the frictional velocity, u^*, is the only unknown. Assuming a near-bed constant stress layer:

$$u(z) = \frac{u_*}{\kappa} \ln\left(\frac{z}{z_o}\right) \tag{6}$$

where z_o is the height above the bed at which the current goes to zero. The velocities at two different heights (u_1 at z_1 and u_2 at z_2) can be used to solve for u^*:

$$u_* = \frac{(u_2 - u_1)\kappa}{\ln\left(\frac{z_2}{z_1}\right)} \tag{7}$$

The two bottom bins of the ADCP, 1.25 m and 2.25 m above the bed, are used to estimate u^*, which is then substituted into equation (5) to estimate the scale height, l. A time series of l indicates that the bottom boundary layer scale height frequently exceeds the water depth (Figure 15). With a mean value of 65 m and a standard deviation of 50 m, the shallow water column (<30 m) within the HF radar grid is dominated by overlapping boundary layers.

[28] Using the linear model described in equations (1) and (2), u_{cor} and v_{cor} was subtracted from the total transient leaving the uncorrelated variance. The principle components have less energy than the total response, however the structure observed in the total variance of the mixed regime is still evident in the uncorrelated field (Figure 13d). The wind forcing appears to amplify the mixed response but does not drive it. Even without the wind forcing, the spatial structure of the variance remains.

3.4.3. Bottom Topography

[29] Since the entire water column is moving as a frictional layer, the influence of the underlying topography should be evident in the surface currents. There is already an indication of this interaction in the mixed, stratified, and annual fields. To quantify the role of the topography, the along isobath direction was calculated at each HF radar grid point using the depth gradient vector, $\vec{H}$.

$$\vec{H} = \frac{\partial h}{\partial L_x}\hat{i} + \frac{\partial h}{\partial L_y}\hat{j} \tag{8}$$

Where $\hat{i}$ and $\hat{j}$ are unit vectors, h is depth, and $L_x(L_y)$ is the east (north) component of the horizontal scale. By definition the along-isobath direction is orthogonal to $\vec{H}$. Since the small-scale ridge and swale topography common along the United States east coast is on the order of 5 km [*McBride and Moslow*, 1991], this length scale was chosen for this analysis. Equation (8) was solved using finite differences such that $L_x = L_y = 5$ km. The magnitude of the depth gradient at this 5 km scale is characterized by four regions of relatively steep topography over our domain (Figure 16a). Two regions fall along the 20 m isobath, one further offshore along the 25 m isobath, and a final area nearshore associated with the topographic bump. The effect of these regions of steeper topography on the surface current variability of the mixed regime is seen when the major axis of the variability is differenced from the along-isobath direction (Figure 16b). Regions in the coverage with small angular offsets indicate that the current variability tends to be more aligned with the topography compared to regions with larger angular offsets. Over our domain the four regions with relatively steeper topography correspond with regions of smaller angular offsets, indicating that the current variability tends to be more aligned with the steeper topography than the flatter topography (Figure 16b). There is a clear trend in which the angular offset is more variable over topography with small slopes (Figure 16c). As the topography steepens, the variability in the angular offset

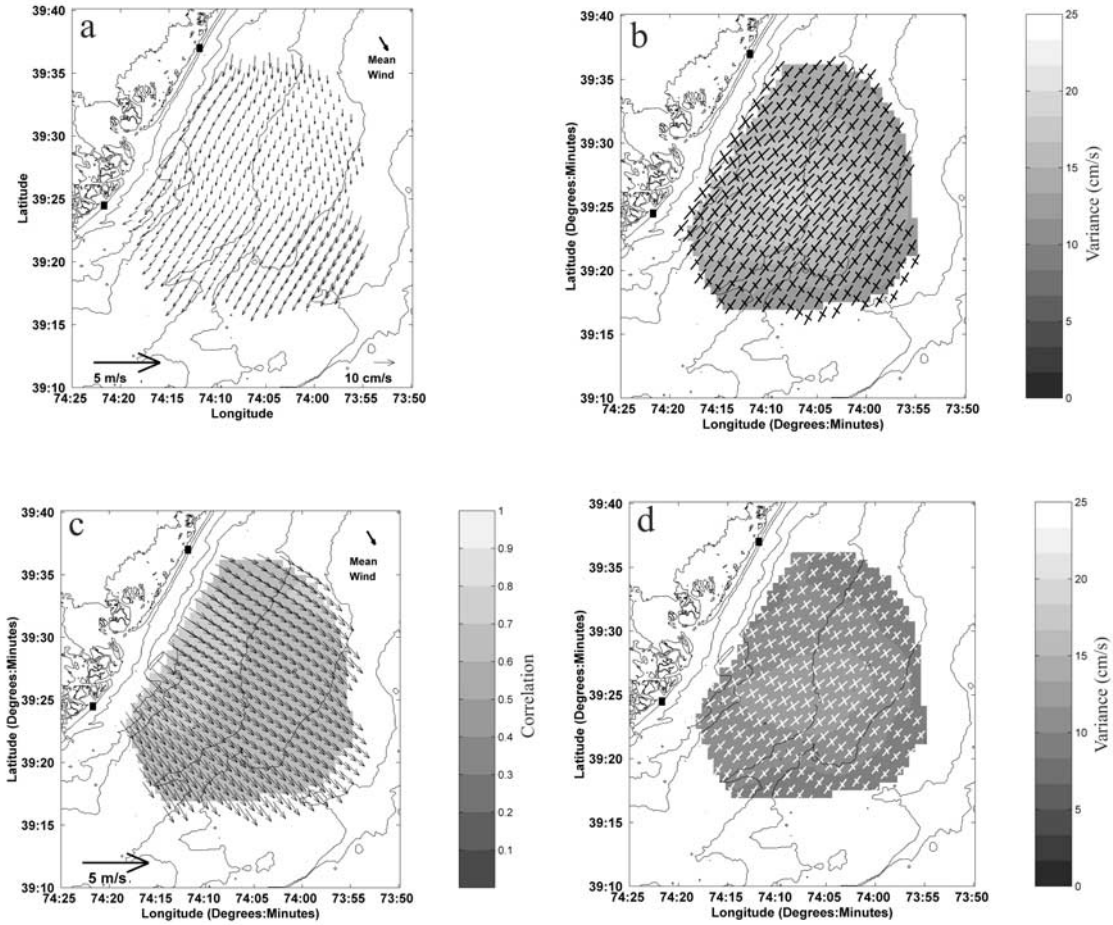

Figure 13. (a) The mean mixed regime response. The mean mixed wind measured at the field station (upper right), the current scale (lower right), and wind scale (lower left) are also shown. (b) Principle components of the mixed regime transient response. (c) The magnitude of the complex correlation of the mixed regime transient response with the local winds is shaded. The angle between the mean wind (upper right) each grid point (black vectors) indicates the offset between the highest correlated current and wind. (d) Variance of the uncorrelated current component of the mixed regime transient response.

decreases and favors smaller angles. The current response of the mixed regime is closely linked to this 5 km scale topography. At this scale the angular offset between the current variability and the topography tends to be more random over areas of relatively flat topography and more aligned over areas with relatively steep topography.

4. Discussion and Conclusions

[30] Throughout the year the influence of topography was observed in the surface current response. Over annual timescales the southward current is steered around a topographic bump seen along the nearshore edge of the data coverage. Using finite difference on the mean surface current fields, vorticity fields were calculated for the mixed, stratified, upwelling and downwelling regimes. In both the mixed and stratified mean flows, there is a ridge of positive vorticity to the north of the bump and a ridge of negative vorticity to the south (Figure 17). This pattern is also seen in the upwelling (Figure 17c) and downwelling (Figure 17d) subsets of the stratified regime. While this pattern persists throughout the year, there is evidence of a seasonal dependence. During the stratified regime, in both the upwelling and downwelling regimes, the magnitude of the vorticity is higher and concentrated closer to the coast than during the mixed regime. Stratification appears to shorten the horizontal length scale in which the influence of the bump is felt, but the response is more intense. When the water column is mixed, the vorticity associated with the bump extends further offshore and is much weaker.

[31] During the summer stratified season the surface layer is very highly correlated with the local wind forcing, with the highest correlated currents at the surface to the right of the wind. The vertical structure of the correlation shows a two-layer system in which the surface layer flows to the right of the wind and the bottom layer flows to the left. Both the forcing and the response show that the stratified regime is dominated by upwelling/downwelling events. During these events the surface current response to the wind is dependent on both local topography and stratification. In contrast, the mixed regime forcing and response is much more variable. The response tends to be aligned with the coast even though the stronger wind fields no longer favor the alongshore direction. The mean flow during

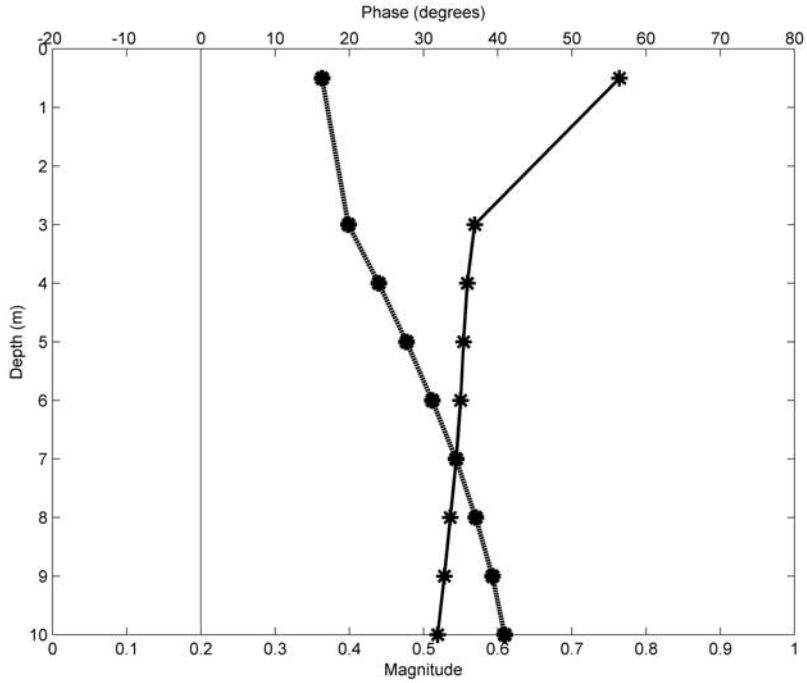

Figure 14. Magnitude (thick) and phase (dashed) of the complex correlation between the vertical current profile and the local wind forcing during the mixed regime. The markers indicate the centers of the measurement bins for the ADCP and CODAR (surface). Negative phase indicates that the highest correlated current is to the right of the wind. The thin line indicates zero phase.

mixed conditions resembles the annual mean having a general flow toward the southwest with perturbations around the local topography. The vertical structure of the correlation shows a single layer in which the most wind-correlated current is to the left of the wind throughout the water column. The left offset of the most correlated current increases with depth. The frictional length scale calculated throughout this period indicates that the entire water column is composed of a single frictional layer. As a single layer, the surface response is strongly influenced by the local topography, especially over those regions in which the slope exceeds 1.3 m/km.

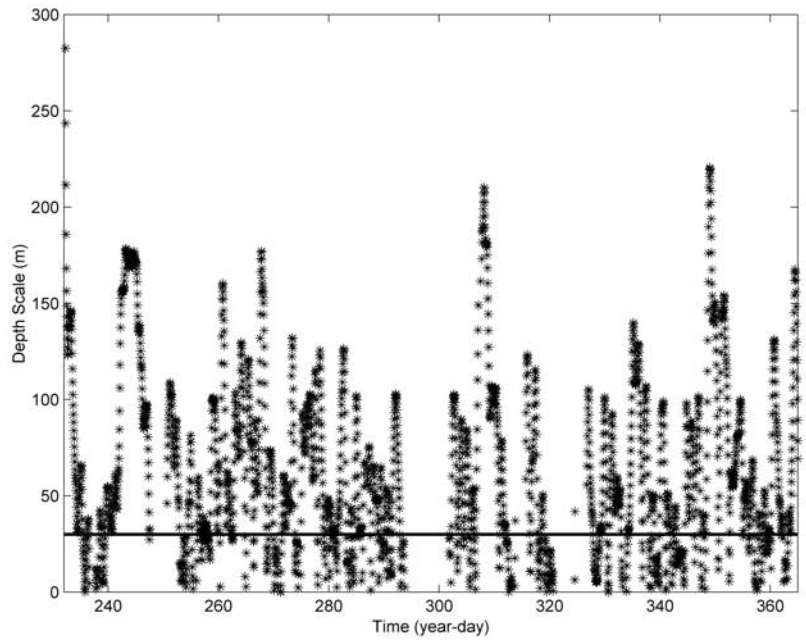

Figure 15. Time series of frictional layer thickness, *l*, defined by equation (3.5). For reference, the solid black line indicates the 30 m isobath.

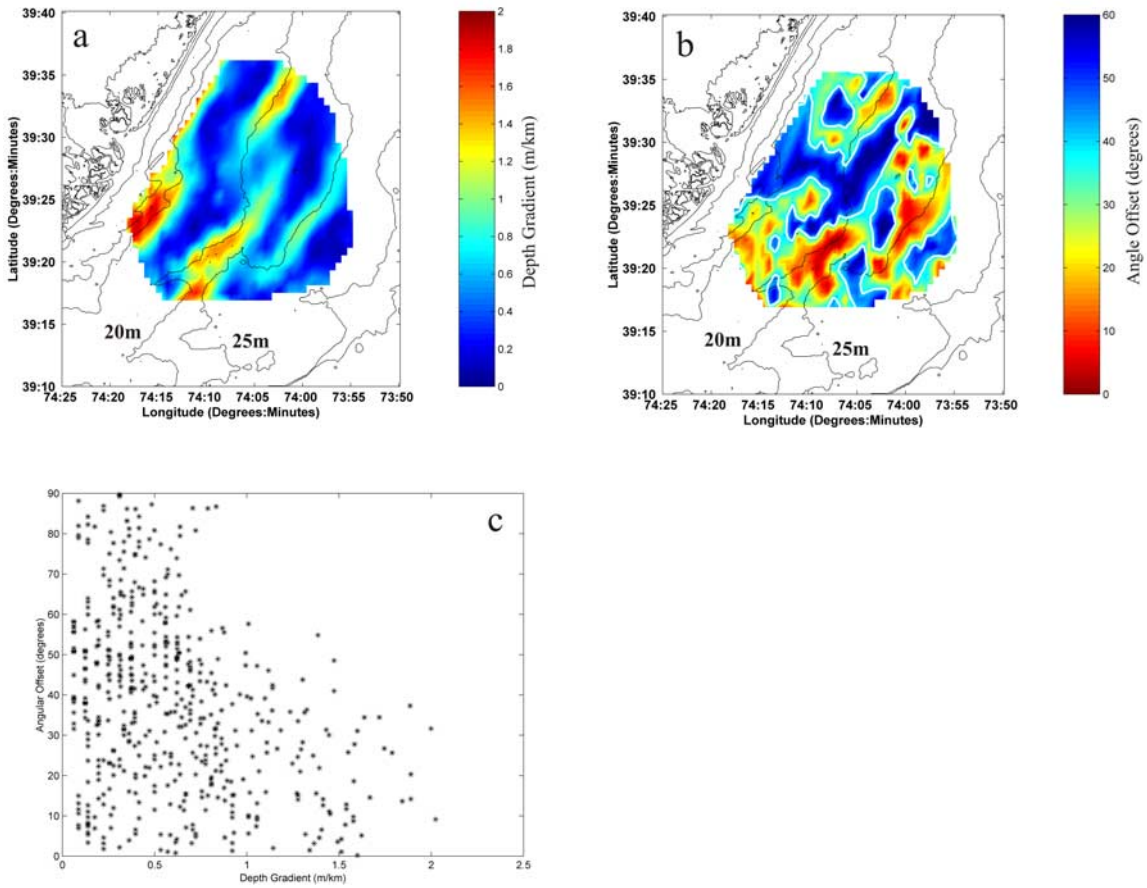

Figure 16. (a) The magnitude of the 5 km scale depth gradient. The 20 m and 25 m isobaths are also labeled. (b) The difference between the 5 km scale along-isobath direction and the major axis of the mixed residual response (Figure 13d). (c) Scatterplot of the depth gradient (Figure 16a) and angular offset between the along-isobath direction and the major axis of the mixed residual response (Figure 16b).

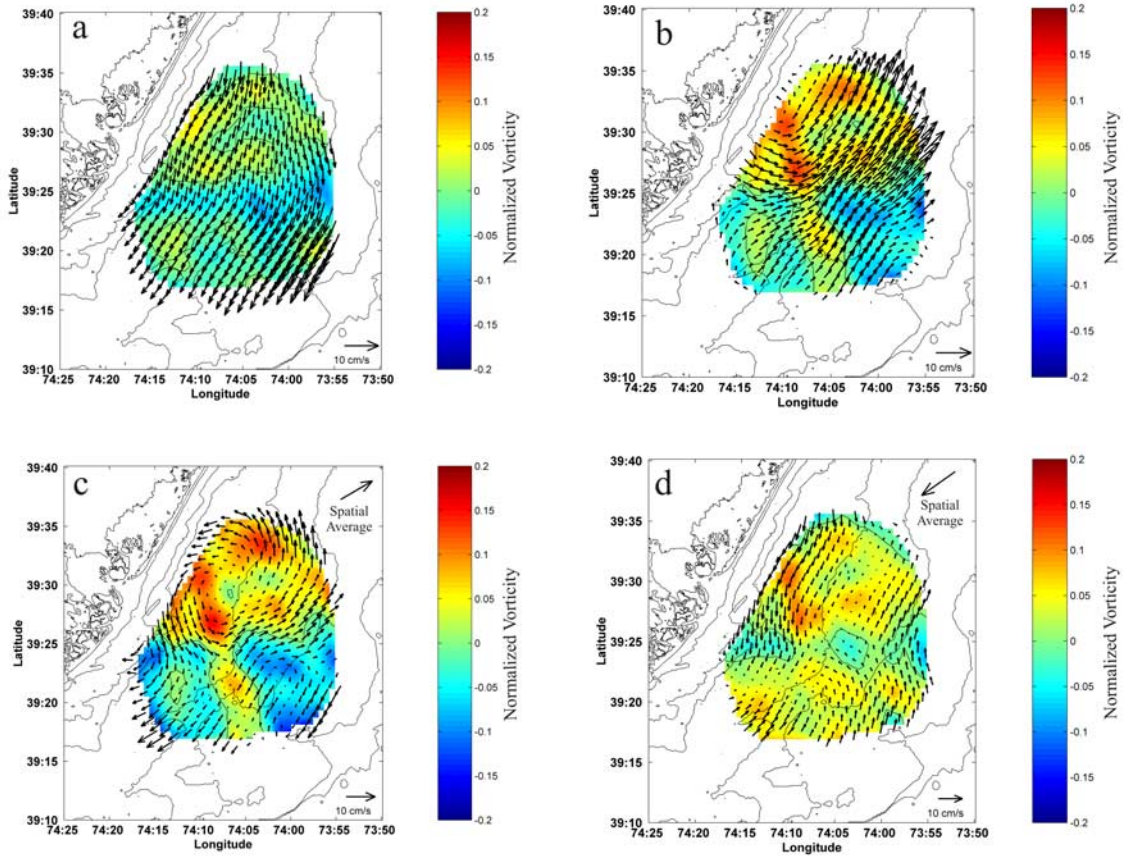

Figure 17. Relative vorticity normalized by the local Coriolis parameter for the mean (a) mixed, (b) stratified, (c) upwelling stratified, and (d) downwelling stratified regimes. The vector fields in Figures 17a and 17b are the temporal mean. The vector fields in Figures 17c and 17d are the difference between the temporal mean at each grid point and the spatial mean (upper right).

[32] Stratification clearly influences the response of the surface currents to local forcing. The results suggest that the complex correlation of the wind with the current could be a proxy of the strength of the stratification. If the water column is stratified, the highly correlated surface layer motion is shifted to right of the wind and, in some locations, also influenced by the underlying topography. If the water column is mixed, the less correlated response is shifted to the left of the wind and is significantly influenced by the underlying topography, especially where the depth gradients are at maximum.

[33] **Acknowledgments.** We would like to thank Dale Haidvogel, Jeff Paduan, Matt Oliver, and two anonymous reviewers for their comments and review. This work was funded by the Office of Naval Research (N00014-97-1-0797, N00014-99-1-0196, N00014-00-1-0724, N00014-02-1-0917), the National Ocean Partnership Program (N00014-97-1-1019, N000-14-98-1-0815), and the great state of New Jersey. ADCP data provided by the Mid-Atlantic Bight National Undersea Research Center with additional support from the National Science Foundation.

References

Austin, J. A. (1999), The role of the alongshore wind in the heat balance of the North Carolina inner shelf, *J. Geophys. Res.*, *104*, 18,187–18,203.

Barrick, D. E. (1972), First-order theory and analysis of mf/hf/vhf scatter from the sea, *IEEE Trans. Antennas Propag.*, *AP-20*, 2–10.

Barrick, D. E., M. W. Evens, and B. L. Weber (1977), Ocean surface currents mapped by radar, *Science*, *198*, 138–144.

Barth, J. A. (1994), Stability of a coastal upwelling front: 2. Model results and comparisons with observations, *J. Geophys. Res.*, *99*, 10,857–10,883.

Battisti, D. S., and A. J. Clarke (1982), A simple method for estimating barotropic tidal currents on the continental margins with specific application to the M2 tide off the Atlantic and Pacific coasts of the United States, *J. Phys. Oceanogr.*, *12*, 8–16.

Beardsley, R. C., and W. C. Boicourt (1981), On estuarine and continental-shelf circulation in the Middle Atlantic Bight, in *Evolution in Physical Oceanography*, edited by B. A. Warren and C. Wunsch, pp. 198–233, MIT Press, Cambridge, Mass.

Beardsley, R. C., and D. B. Haidvogel (1981), Model studies of wind-driven transient circulation in the Middle Atlantic Bight, part 1: Adiabatic boundary conditions, *J. Phys. Oceanogr.*, *11*, 355–375.

Beardsley, R. C., and S. J. Lentz (1987), The Coastal Ocean Dynamics Experiment collection: An introduction, *J. Geophys. Res.*, *92*, 1455–1463.

Beardsley, R. C., and C. D. Winant (1979), On the mean circulation in the Mid-Atlantic Bight, *J. Phys. Oceanogr.*, *9*, 612–619.

Beardsley, R. C., W. C. Boicourt, and D. V. Hansen (1976), Physical oceanography of the Middle Atlantic Bight, *Limnol. Oceanogr. Spec. Symp.*, *2*, 20–34.

Bernstein, R. L. (1982), Sea surface temperature estimation using the NOAA-6 advanced very high resolution radiometer, *J. Geophys. Res.*, *87*, 9455–9465.

Bigelow, H. B. (1933), Studies of the waters on the continental shelf, Cape Cod to Chesapeake Bay. I. The cycle of temperature, *Pap. Phys. Oceanogr. Meteorol.*, *2*, 135 pp.

Bigelow, H. B., and M. Sears (1935), Studies of the waters on the continental shelf, Cape Cod to Chesapeake Bay. II. Salinity, *Pap. Phys. Oceanogr. Meteorol.*, *4*, 94 pp.

Brink, K. H. (1997), Observational coastal oceanography, paper presented at National Science Foundation OCE Workshops, Natl. Sci. Found., Monterey, Calif.

Brink, K. H., D. Halpern, and R. L. Smith (1980), Circulation in the Peruvian upwelling system near 15°S, *J. Geophys. Res.*, *85*, 4036–4048.
Chant, R. J. (2001), Evolution of near-inertial waves during an upwelling event on the New Jersey inner shelf, *J. Phys. Oceanogr.*, *31*, 746–763.
Chapman, D. C., and R. C. Beardsley (1989), On the origin of shelf water in the Middle Atlantic Bight, *J. Phys. Oceanogr.*, *19*, 384–391.
Chapman, R. D., L. K. Shay, H. C. Graber, J. B. Edson, A. Karachintsev, C. L. Trump, and D. B. Ross (1997), On the accuracy of HF radar surface current measurements: Intercomparisons with ship-based sensors, *J. Geophys. Res.*, *102*, 18,737–18,748.
Crombie, D. D. (1955), Doppler spectrum of sea echo at 13.56 Mc/s, *Nature*, *175*, 681–682.
Davis, R. E., and P. S. Bogden (1989), Variability on the California shelf forced by local and remote winds during the Coastal Ocean Dynamics Experiment, *J. Geophys. Res.*, *94*, 4763–4783.
Forristall, G. Z., R. C. Hamilton, and V. J. Cardone (1977), Continental shelf currents in tropical storm Delia: Observations and theory, *J. Phys. Oceanogr.*, *7*, 532–546.
Glenn, S. M. (1983), A continental shelf bottom boundary layer model: The effect of waves, currents, and a moveable bed, Ph.D. diss., 237 pp., Woods Hole Oceanogr. Inst./Mass. Inst. of Technol. Joint Program, Woods Hole.
Glenn, S. M., M. F. Crowley, D. B. Haidvogel, and Y. T. Song (1996), Underwater observatory captures coastal upwelling events off New Jersey, *Eos Trans. AGU*, *77*, 233–236.
Glenn, S. M., W. Boicourt, B. Parker, and T. D. Dickey (2000), Operational observation networks for ports, a large estuary and an open shelf, *Oceanography*, *13*, 12–23.
Grassle, J. F., S. M. Glenn, and C. von Alt (1998), Ocean observing systems for marine habitats, *OCC '98 Proceedings*, Mar. Technol. Soc., Baltimore, Md.
Halpern, D. (1976), Structure of a coastal upwelling event observed off Oregon during July 1973, *Deep Sea Res.*, *23*, 495–508.
Halpern, D. (1977), Description of wind and of upper ocean currents and temperature variation on the continental shelf off northwest Africa during March and April 1977, *J. Phys. Oceanogr.*, *7*, 422–430.
Hicks, D. C., and J. R. Miller (1980), Meteorological forcing and bottom water movement off the northern New Jersey coast, *Estuarine Coastal Sci.*, *II*, 563–571.
Houghton, R. W., R. Schlitz, R. C. Beardsley, B. Butman, and J. L. Chamberlin (1982), The Middle Atlantic Bight cold pool: Evolution of the temperature structure during summer 1979, *J. Phys. Oceanogr.*, *12*, 1019–1029.
Kohut, J. T., and S. M. Glenn (2003), Improving HF radar surface current measurements with measured antenna beam patterns, *J. Atmos. Oceanic Technol.*, *20*, 1303–1316.
Long, C. E. (1981), A simple model for time-dependent stably stratified turbulent boundry layers, *Spec. Rep. 95*, 170 pp., Dep. of Oceanogr., Univ. of Washington, Seattle, Wa.
McBride, R. A., and T. F. Moslow (1991), Origin, evolution, and distribution of shoreface sand ridges, Atlantic inner shelf, U.S.A., *Mar. Geol.*, *97*, 57–85.
Miller, A. R. (1952), A pattern of surface coastal circulation inferred from surface salinity-temperature data and drift bottle recoveries, *WHOI Tech. Rep. 52–28*, 14 pp., Woods Hole Oceanogr. Inst., Woods Hole, Mass.
Moores, C. N. K., J. Fernandez-Partagas, and J. F. Price (1976), Meteorological forcing fields of the New York Bight (first year's progress report), *Tech. Rep. TR76–8*, Rosenstiel School of Mar. and Atmos. Sci., Univ. of Miami, Miami, Fla.
Münchow, A., and R. J. Chant (2000), Kinematics of inner shelf motions during the summer stratified season off New Jersey, *J. Phys. Oceanogr.*, *30*, 247–267.
Narimousa, S., and T. Maxworthy (1987), Coastal upwelling on a sloping bottom: The formation of plumes, jets and pinched-off cyclones, *J. Fluid Mech.*, *176*, 169–190.
Ou, H. W., R. C. Beardsley, D. Mayer, W. C. Boicourt, and B. Butman (1981), An analysis of subtidal fluctuations in the Middle Atlantic Bight, *J. Phys. Oceanogr.*, *11*, 1383–1392.
Saunders, P. M. (1977), Wind stress on the ocean over the eastern continental shelf of North America, *J. Phys. Oceanogr.*, *7*, 555–566.
Schofield, O., T. Bergmann, W. P. Bissett, F. Grassle, D. Haidvogel, J. Kohut, M. Moline, and S. Glenn (2001), The long term ecosystem observatory: An integrated coastal observatory, *IEEE J. Oceanic Eng.*, *27*, 146–154.
Smith, J. D., and C. E. Long (1976), The effect of turning in the bottom boundary layer on continental shelf sediment transport, *Mem. Soc. R. Sci. Liége Coll. 6°*, *X*, 369–396.
Song, Y. T., D. B. Haidvogel, and S. M. Glenn (2001), Effects of topographic variability on the formation of upwelling centers off New Jersey: A theoretical model, *J. Geophys. Res.*, *106*, 9223–9240.
Stewart, R. H., and J. W. Joy (1974), HF radio measurement of surface currents, *Deep Sea Res.*, *21*, 1039–1049.
Svedrup, H. U., M. W. Johnson, and R. H. Fleming (1942), *The Oceans: Their Physics, Chemistry, and General Biology*, 1087 pp., Prentice-Hall, Old Tappan, N. J.
Walford, L. A., and R. I. Wicklund (1968), Monthly sea temperature structure from the Florida Keys to Cape Cod, *Serial Atlas of the Marine Environment*, folio 15, Am. Geogr. Soc. of New York, New York.
Yankovski, A. E., and R. W. Garvine (1998), Subinertial dynamics on the inner New Jersey shelf during the upwelling season, *J. Phys. Oceanogr.*, *28*, 2444–2458.

J. T. Kohut, S. M. Glenn, and R. J. Chant, Institute of Marine and Coastal Sciences, Rutgers University, New Brunswick, NJ, USA. (kohut@imcs.rutgers.edu)